An in situ high-throughput screen identifies inhibitors of intracellular *Burkholderia pseudomallei* with therapeutic efficacy

Philip L. Bulterys[a,b,c,1], Isabelle J. Toesca[c], Michael H. Norris[d,e], Jeffrey P. Maloy[c], Sorel T. Fitz-Gibbon[f], Bryan France[g], Babak Toffig[g], Marco Morselli[f], Nawarat Somprasong[e,h], Matteo Pellegrini[f,g,i], Herbert P. Schweizer[e,h], Apichai Tuanyok[d,e], Robert Damoiseaux[g,j], Christopher T. French[c,g,2], and Jeff F. Miller[b,c,g,2]

[a]University of California, Los Angeles–California Institute of Technology Medical Scientist Training Program, David Geffen School of Medicine, University of California, Los Angeles, CA 90095; [b]Molecular Biology Institute, University of California, Los Angeles, CA 90095; [c]Department of Microbiology, Immunology, and Molecular Genetics, University of California, Los Angeles, CA 90095; [d]Department of Infectious Diseases and Immunology, College of Veterinary Medicine, University of Florida, Gainesville, FL 32611; [e]Emerging Pathogens Institute, University of Florida, Gainesville, FL 32611; [f]Department of Molecular, Cell, and Developmental Biology, University of California, Los Angeles, CA 90095; [g]California NanoSystems Institute, University of California, Los Angeles, CA 90095; [h]Department of Molecular Genetics and Microbiology, University of Florida, Gainesville, FL 32611; [i]Institute of Genomics and Proteomics, University of California, Los Angeles, CA 90095; and [j]Department of Molecular and Medical Pharmacology, University of California, Los Angeles, CA 90095

Contributed by Jeff F. Miller, July 13, 2019 (sent for review April 15, 2019; reviewed by Yunn-Hwen Gan and John J. Mekalanos)

***Burkholderia pseudomallei* (*Bp*) and *Burkholderia mallei* (*Bm*) are Tier-1 Select Agents that cause melioidosis and glanders, respectively. These are highly lethal human infections with limited therapeutic options. Intercellular spread is a hallmark of *Burkholderia* pathogenesis, and its prominent ties to virulence make it an attractive therapeutic target. We developed a high-throughput cell-based phenotypic assay and screened ∼220,000 small molecules for their ability to disrupt intercellular spread by *Burkholderia thailandensis*, a closely related BSL-2 surrogate. We identified 268 hits, and cross-species validation found 32 hits that also disrupt intercellular spread by *Bp* and/or *Bm*. Among these were a fluoroquinolone analog, which we named burkfloxacin (BFX), which potently inhibits growth of intracellular *Burkholderia*, and flucytosine (5-FC), an FDA-approved antifungal drug. We found that 5-FC blocks the intracellular life cycle at the point of type VI secretion system 5 (T6SS-5)-mediated cell–cell spread. Bacterial conversion of 5-FC to 5-fluorouracil and subsequently to fluorouridine monophosphate is required for potent and selective activity against intracellular *Burkholderia*. In a murine model of fulminant respiratory melioidosis, treatment with BFX or 5-FC was significantly more effective than ceftazidime, the current antibiotic of choice, for improving survival and decreasing bacterial counts in major organs. Our results demonstrate the utility of cell-based phenotypic screening for Select Agent drug discovery and warrant the advancement of BFX and 5-FC as candidate therapeutics for melioidosis in humans.**

Burkholderia pseudomallei | melioidosis | type 6 secretion system (T6SS) | small molecule | drug discovery

Burkholderia pseudomallei (*Bp*) and *Burkholderia mallei* (*Bm*), the etiologic agents of melioidosis and glanders, respectively, are highly infectious gram-negative bacteria for which limited therapeutic options exist. *Bp* normally inhabits the rhizosphere (1, 2) and can be acquired by humans and other mammals via inhalation, ingestion, or percutaneous inoculation (3, 4). Individuals regularly exposed to soil and water in endemic areas are disproportionately affected. The severity of disease varies from chronic infection mimicking tuberculosis to acute, florid sepsis. Clinical management is complicated by antibiotic resistance (5–8), and mortality rates are high despite appropriate diagnosis and treatment (9). *Bm* is an evolutionary descendent of *Bp* (10) with a restricted host range that primarily includes solid-ungulates, although it can also cause life-threatening zoonotic infections in humans (11, 12). In light of their low infectious doses, high lethality, extensive antibiotic resistance, and the lack of protective vaccines, *Bm* and *Bp* are classified as Tier 1 Select Agent pathogens. Concern over malign release against civilian or military targets is heightened in light of their historical use as bioweapons (13, 14). A third, less-pathogenic member of the *B. pseudomallei* complex (*Bp* complex), *B. thailandensis* (*Bt*), shares highly conserved virulence mechanisms with its pathogenic relatives, making it a useful BSL-2 surrogate (15–17).

Although the true global burden of melioidosis is unknown, recent estimates suggest that *Bp* is endemic in at least 79 countries and is responsible for 165,000 annual human infections, of which 54% are fatal (18). Highly endemic areas include northeast Thailand, where *Bp* is the leading cause of community-acquired bacteremia, and the Northern Territory of Australia, where *Bp* is the most common cause of fatal community-acquired bacteremic pneumonia (19–21). The current treatment regimen for melioidosis consists of an initial parenteral phase lasting 10 to

Significance

***Burkholderia pseudomallei*, the etiologic agent of melioidosis, is an environmental organism that inhabits tropical soils and kills an estimated 90,000 people each year. Caused by an intracellular and often drug-resistant pathogen, melioidosis is notoriously difficult to treat, with mortality rates approaching 50% in some settings despite appropriate diagnosis and clinical management. Using a high-throughput, cell-based phenotypic screen we have discovered 2 antibiotic candidates with improved in vivo efficacy compared to the current standard of care: a fluoroquinolone analog, burkfloxacin, and an FDA-approved antifungal drug, flucytosine. As a widely used antifungal with a well-known safety profile, the potential to repurpose flucytosine for treating melioidosis may represent a rapid route to clinical translation.**

Author contributions: P.L.B., I.J.T., R.D., C.T.F., and J.F.M. designed research; P.L.B., I.J.T., M.H.N., S.T.F.-G., B.F., B.T., and M.M. performed research; I.J.T., M.H.N., J.P.M., S.T.F.-G., B.F., B.T., M.M., N.S., M.P., H.P.S., A.T., R.D., C.T.F., and J.F.M. contributed new reagents/analytic tools; P.L.B., I.J.T., M.H.N., S.T.F.-G., C.T.F., and J.F.M. analyzed data; and P.L.B., C.T.F., and J.F.M. wrote the paper.

Reviewers: Y.-H.G., National University of Singapore; and J.J.M., Harvard University.

The authors declare no conflict of interest.

[1]Present address: Department of Pathology, Stanford University, Stanford, CA 94305.

[2]To whom correspondence may be addressed. Email: ctfrench@ucla.edu or jfmiller@g.ucla.edu.

This article contains supporting information online at www.pnas.org/lookup/suppl/doi:10.1073/pnas.1906388116/-/DCSupplemental.

Published online August 22, 2019.

14 d aimed at preventing death, followed by an oral eradication phase lasting >3 mo aimed at preventing relapse. Ceftazidime and carbapenems are the mainstays for acute phase therapy, while trimethoprim-sulfamethoxazole (cotrimoxazole) or amoxicillin-clavulanic acid (coamoxiclav) are the choices for eradication phase therapy (4, 22). The efficacy of current treatment regimens is limited, however, by intrinsic and acquired antibiotic resistance (8, 23–26). The consequences of naturally occurring disease, the potential for nefarious use, the lack of effective vaccines, and drug resistance make the development of new countermeasures a high priority.

Bp complex species can parasitize mammalian cells, and their ability to replicate intracellularly and spread from cell to cell is an essential virulence trait (4). Following entry by phagocytosis or invasion, bacteria escape from endocytic vesicles using the Bsa type III secretion system ($T3SS_{Bsa}$) (27, 28) (Fig. 1). Bacteria then multiply in the cytoplasm, move through the cytosol by BimA-mediated actin polymerization (29), and spread to neighboring cells by a process involving membrane fusion (28, 30), creating a portal for direct passage of bacteria into neighboring cytosolic compartments (31). Membrane fusion requires the activity of type VI secretion system 5 (T6SS-5), 1 of 6 T6SSs encoded in *Bp* complex genomes (31–33), and multiple cell fusion events result in the formation of large multinucleate cells (MNCs) which eventually lyse to form lesions (i.e., plaques) on cell monolayers (28).

Host cell fusion by *Bp* complex species differs significantly from multinucleated giant cell (MGC) formation observed in mycobacterial infections or other granulomatous diseases. In these settings, MGCs develop by cytokine-mediated activation of a fusion program that is intrinsic to monocytes and macrophages and can be reproduced in vitro in the absence of bacteria by the addition of cytokines alone (34). In contrast, cell fusion by *Bp*, *Bt*, and *Bm* results from the activity of a bacterial virulence determinant, T6SS-5, a contractile nanotube evolutionarily related to phage tails that is embedded in the cell envelope and fires outward (35–39). According to the current model (Fig. 1), encounters between intracellular *Burkholderia* and the plasma membrane lead to T6SS-5 contraction, firing of a bacterially encoded fusogenic protein (VgrG5) across the bacterial envelope and through the plasma membranes of the infected cell and an adjacent cell, causing local deformation and merging of opposing bilayers (28, 31). *Burkholderia* are able to fuse a wide range of cell types in vitro, including epithelial cells, endothelial cells, fibroblasts, monocytes, and macrophages (40), and fusion ability correlates with virulence by *Bp* and *Bm* (32, 41–43).

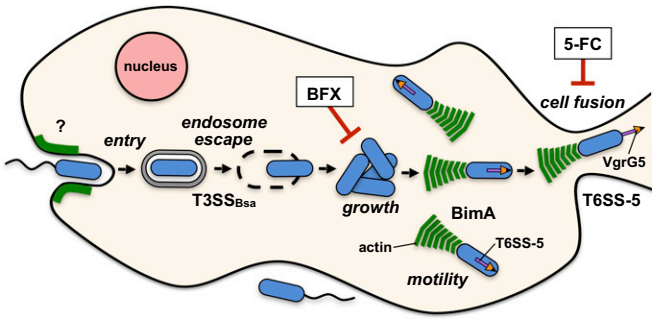

Fig. 1. Intracellular life cycle of *B. pseudomallei* complex species, showing points of inhibition by 2 newly discovered small-molecule inhibitors, burkfloxacin (BFX) and flucytosine (5-FC). Diagram of the *Burkholderia* intercellular life cycle, illustrating the ability to invade mammalian cells, escape from endosomes/phagosomes, locomote in the cytosol by polymerizing host actin, replicate intracellularly, and fuse host cell membranes by a T6SS-5–dependent mechanism (31). Two priority compounds, BFX and 5-FC, were found to inhibit intracellular replication and cell fusion, respectively.

Target-based screening campaigns against gram-negative bacteria have been largely unsuccessful due to the inability of many small molecules to penetrate the bacterial outer membrane (44–46). Furthermore, prior efforts to develop therapeutics against *Burkholderia* have shown that despite having activity in vitro, compounds are often ineffective in vivo due to the ability of *Bp* and *Bm* to survive and replicate intracellularly (47). With these limitations in mind, we developed a cell-based phenotypic screen for small-molecule inhibitors of intracellular *Burkholderia* that are actively replicating within and spreading between mammalian cells. Our high-throughput (HT) assay comprehensively assesses the entire *Burkholderia* intercellular life cycle, including the critical step of cell–cell fusion. We screened ~220,000 small molecules for their ability to disrupt intercellular spread by *Bt* and validated positive hits using the BSL-3 pathogens *Bp* and *Bm*. This strategy identified 32 compounds that disrupt the intracellular life cycle of *Bp* and/or *Bm*. We describe the mechanistic characterization of 2 of our most potent inhibitors, which hold promise as therapeutic countermeasures against melioidosis.

Results

A High-Throughput Phenotypic Screen Identifies Small-Molecule Inhibitors of *Burkholderia* Intercellular Spread. The cell fusion assay shown in Fig. 2*A* was adapted for high-throughput screening by seeding eGFP-expressing HEK293 cells into 384-well plates pinned with a library of small molecules, infecting cells with *Burkholderia*, and imaging 18 to 22 h later using laser scanning cytometry to assess the relative abundance and size of plaques (Fig. 2 *B* and *C*). Given that the readout results from cell fusion mediated by intracellular bacteria, the assay is capable of identifying compounds that inhibit any step of the intracellular infection pathway, have relatively low toxicity against mammalian cells, and are capable of penetrating both the host cell plasma membrane and the gram-negative cell envelope.

A curated small-molecule library was screened for inhibitory activity against intracellular *Bt* strain E264 utilizing the facilities of the University of California, Los Angeles (UCLA), Molecular Screening Shared Resource (MSSR). Fig. 2*C* shows a pilot screen using an FDA-approved sublibrary of 1,120 compounds, demonstrating the ability to identify known (trimethoprim) as well as new inhibitors. Screening efforts were then scaled to accommodate >220,000 compounds. Over the course of the screen, control wells yielded negligible false-positive (0%) and false-negative (0.0091%) hit rates. An initial set of 268 compounds was found to inhibit plaque formation by *Bt* E264, yielding a conservative primary hit rate of 0.0012. Validation was conducted using *Bt* E264, *Bp* 1026b (Thai clinical isolate), and *Bm* 23344 (human isolate), resulting in 114 (43%) validated compounds that were binned according to species activity (Fig. 2*D*). Of these, 4 compounds, including 3 known antibiotics and 1 molecule which we named burkfloxacin (BFX), were found to consistently inhibit plaque formation by all 3 organisms. Seven compounds, including 4 known antibiotics, inhibited plaque formation by *Bm* and *Bp*, and 4 compounds were specific for *Bm* only, including monensin and the antimalarial drug artemisinin. Flucytosine (5-fluorocytosine, 5-FC), an FDA-approved antimycotic, was identified among the hits with activity against *Bp* and *Bt* but not *Bm*. Following validation of activity against intracellular *Burkholderia*, cytotoxicity was assessed in HEK293 cells using an ATP-depletion cell viability assay. Both BFX and 5-FC had no apparent effect on cell viability at concentrations 10-fold higher than the IC_{100} (*SI Appendix*, Table S1) and were prioritized for follow-up studies.

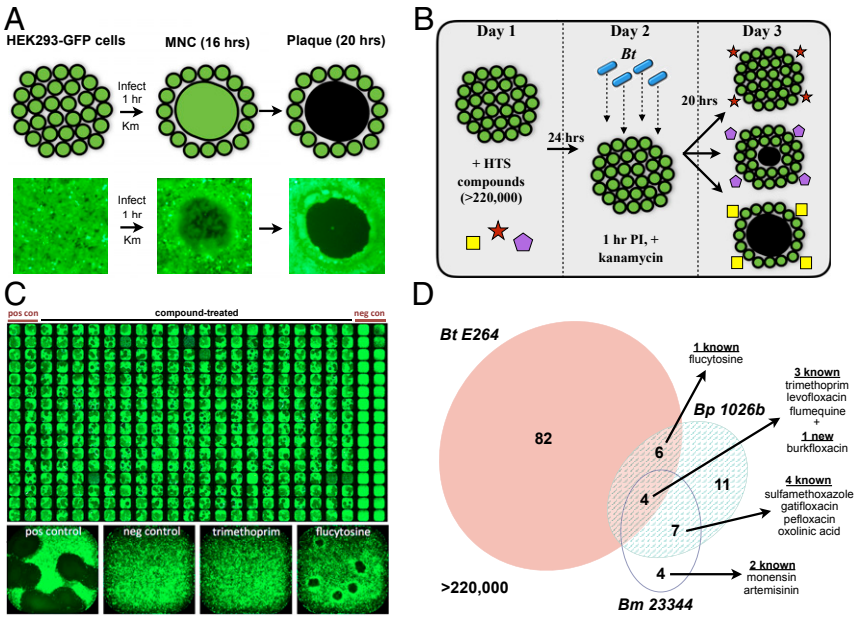

Fig. 2. High-throughput screening for small-molecule inhibitors of *Burkholderia* intercellular spread. (*A*) Cell fusion assay with example well images. HEK293-GFP cell monolayers were infected at a multiplicity of infection of 0.01, treated with 125 μg/mL kanamycin after 1 h to prevent extracellular growth, and incubated for 20 h. *Burkholderia*-driven membrane fusion leads to multinucleate cells that eventually lyse to form plaques. (*B*) Schematic of the high-throughput phenotypic small-molecule screen. The 384-well plates containing cell culture media were pinned with small molecules dissolved in DMSO for a final concentration of 5 μM. Cells were then seeded onto plates (35,000 per well), incubated for 24 h, then subjected to cell fusion assays and evaluated for plaque formation. Red stars represent compounds that cause complete inhibition, purple pentagrams indicate partial inhibition (small plaque phenotype as shown or reduced number of plaques), and yellow squares represent no inhibitory effect. (*C*) Example 384-well plate image from screening of an FDA-approved drug library (Prestwick) at 5 μM concentration, with *Bt E264*. (*Lower*) The enlarged image of a positive control well (DMSO-treated and infected), negative control well (uninfected), and wells containing trimethoprim and flucytosine (5-FC). (*D*) A proportional Venn diagram showing the number of small molecules that reproducibly inhibited intercellular spread by *Bt*, *Bp*, and/or *Bm*. Of the 268 primary hits originally identified during high-throughput screening against *Bt*, 92 reproducibly inhibited *Bt* intercellular spread, and 32 reproducibly inhibited intercellular spread by *Bp* and/or *Bm*. Known drugs identified in the screen are listed by category in the Venn diagram and include numerous FDA-approved antibiotics, as well as the antimalarial artemisinin, which showed activity against *Bm*. Hit validation experiments with *Bt*, *Bp*, and *Bm* were performed in 384-well plate format with at least 3 technical and 2 biological replicates. MNC, multinucleate cell; HTS, high-throughput screen; PI, postinfection.

BFX Potently Inhibits Growth of Intracellular *Burkholderia*. BFX (Fig. 3*A*) is a morpholinated fluoroquinolone analog originally synthesized in 1980 by Koga et al. (48). In this and a subsequent study (49), it was found to have in vitro activity against a limited panel of bacterial species and a favorable toxicity profile. We confirmed that BFX is active against other gram-negative organisms in vitro, showing similar potency to the widely used fluoroquinolone, ciprofloxacin (Cip), against *Escherichia coli* ATCC 25922 and *Pseudomonas aeruginosa* ATCC 27853 (*SI Appendix*, Table S2). We also confirmed that BFX, like Cip, functions as a canonical fluoroquinolone by demonstrating its ability to inhibit the negative DNA supercoiling activity of *E. coli* DNA gyrase (Fig. 3*B*).

As shown in Fig. 3*C*, BFX results in near-complete inhibition of plaque formation by *Bt* and *Bp* at a concentration of 0.5 μM. In the intracellular growth experiment in Fig. 3*D*, bacteria replicate exponentially in the absence of drug until ∼16 h, when membrane damage accumulates to an extent sufficient to expose intracellular bacteria to bactericidal levels of kanamycin present in the media. In contrast, intracellular growth is ablated following treatment with BFX. When compared to Cip present at the same concentration (1.0 μm), BFX resulted in a 7-fold reduction in colony forming units (CFU) at the point of maximal intracellular growth (16 h, Fig. 3*E*), and in plaque assays, BFX inhibited cell–cell spread at an 8-fold lower concentration compared to Cip (*SI Appendix*, Fig. S1). Interestingly, significantly higher doses of BFX (5 μM) were needed to inhibit growth in laboratory medium (Fig. 3*F*), compared to intracellular growth in HEK293 cells (Fig. 3*D*), suggesting that BFX accumulation may occur inside mammalian cells as observed with certain other fluoroquinolones (50).

The FDA-Approved Antifungal, 5-FC, Inhibits Intercellular Spread at the Step of Cell–Cell Fusion. Our screen also identified 5-FC (Fig. 4*A*), an FDA-approved antimycotic, as an inhibitor of plaque formation by *Bt* and *Bp*. Flucytosine is a fluorinated cytosine analog that serves as a first-line therapy for serious fungal infections, such as cryptococcal meningitis (51), and is included in the World Health Organization's List of Essential Medicines (52). In light of its established efficacy as an antifungal agent, we investigated the mechanism of 5-FC activity as an inhibitor of *Burkholderia* cell–cell spread. As shown in Fig. 4*B*, 5-FC inhibits plaque formation by *Bt* and *Bp* in a dose-dependent fashion, as indicated by a decrease in both plaque numbers and size (also see Fig. 2*C*). Flucytosine does not affect bacterial growth in laboratory medium at a concentration that nearly eliminates plaque formation (Fig. 4*C*). Similarly, 5-FC does not prevent growth of intracellular bacteria at concentrations that inhibit plaque formation, although a decrease and delay in attaining peak bacterial numbers is observed (Fig. 4*D*). Plaque formation is inhibited whether 5-FC is added to cells before or after bacterial infection (Fig. 4*E*), indicating an effect on a late intracellular life cycle event. This contrasts with 2 other compounds identified in our screen, Invasion Inhibitor-1 (II-1) and Invasion Inhibitor-2 (II-2), which show strong inhibition of cell–cell spread when added prior to infection but minimal activity when added after infection, as expected for inhibitors of invasion (Fig. 4*E*). For 5-FC, the proportion of cytosolic bacteria associated with actin tails is equivalent in treated and untreated cells (Fig. 4*F*). Importantly, in comparison to the wild-type (WT) strain (Fig. 4*D*), peak intracellular growth levels of a fusion-defective Δ*vgrG5* mutant (31) were not significantly affected by 5-FC (Fig. 4*G*), although we did observe a delay that was similar to that seen with the WT strain (Fig. 4*D*). Since cell fusion allows expansion of the *Burkholderia* replicative niche and facilitates intracellular replication, the lack of a difference in peak numbers for the Δ*vgrG5* mutant with or without 5-FC, together with time of addition data (Fig. 4*E*) and observations of actin polymerization by cytosolic bacteria (Fig. 4*F*), support the hypothesis that 5-FC inhibits a late-stage event in the intracellular life cycle that is required for cell fusion.

To further explore the inhibitory mechanism, we investigated the effects of 5-FC on the expression of virulence loci known to facilitate intracellular survival and cell–cell spread (53). Quantitative RT-PCR measurements of transcripts from genes involved in virulence regulation (*virG* and *bsaN*), endosome

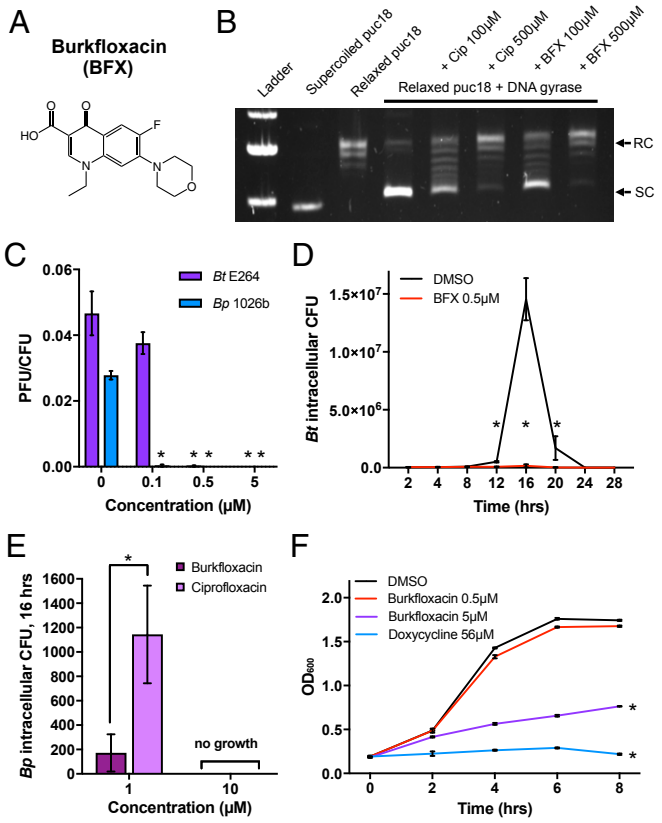

Fig. 3. Identification of a fluoroquinolone, BFX, as a potent inhibitor of *Burkholderia* intracellular replication. (*A*) Chemical structure of BFX (1-ethyl-6-fluoro-7-(4-morpholinyl)-4-oxo-1,4-dihydro-3-quinolinecarboxylic acid). (*B*) BFX inhibited the negative supercoiling activity of *E. coli* DNA gyrase, similarly to Cip. RC, relaxed circular; SC, supercoiled. (*C*) Plaque forming efficiency of *Bt* E264 and *Bp* 1026b at varying concentrations of BFX. BFX treatment resulted in near-complete inhibition of intercellular spread by *Bt* E264 and *Bp* 1026b at a concentration of 0.5 μM. Plaque forming efficiency was assessed by the number of plaque forming units (PFU) per CFU in confluent HEK293 cell monolayers 16 h after infection with a multiplicity of infection (MOI) of 4×10^{-4} (*$P < 0.001$). (*D*) BFX inhibited intracellular replication of *Bt* at a concentration of 0.5 μM. Intracellular bacterial counts were significantly lower in BFX-treated cells compared to DMSO-treated cells at 12, 16, and 20 h after infection (*$P < 0.05$). Intracellular CFUs were determined by treating confluent cell monolayers with 0.5 μM BFX or DMSO, infecting 1 h later with *Bt* at an MOI of 1, adding K_m 1 mg/mL 1 h after infection to kill extracellular bacteria, then lysing monolayers and plating dilutions at predetermined time points (27, 29). (*E*) At a concentration of 1 μM, 7-fold fewer CFU were recovered from BFX-treated cells vs. Cip-treated cells at maximal intracellular growth (16 h postinfection) (*$P < 0.05$). Intracellular CFUs were enumerated by infecting monolayers as described above using an MOI of 1.0. At 16 h postinfection, cells were lysed, and dilutions were plated for CFU determinations. (*F*) BFX did not inhibit in vitro growth of *Bt* in LB-NS at a concentration that robustly inhibits intracellular replication (0.5 μM), but inhibition was observed at a 10-fold higher concentration (5 μM) (*$P < 0.001$). *C–F* show the mean of at least 3 technical replicates, with all error bars representing the SD.

escape (*bsaM* and *bopE*), intracellular motility (*fliC2* and *bimA*), or T6SS-5–dependent membrane fusion (*clpV5* and *vgrG5*) were performed on RNA isolated from HEK293 cells infected with *Bt* E264 in the presence or absence of 5-FC. With treatment, we found a modest (≤4-fold) and variable reduction in the expression of *virG*, *bsaM*, *bimA*, and *vgrG5* and an even smaller effect on *bsaN*, *bopE*, *flic2*, or *clpV5* (Fig. 4*H*). This seemed unlikely to account for the near-complete elimination of plaque formation observed with 5-FC at the same concentration (25 μm), and more likely due to secondary growth effects resulting from the lack of efficient cell fusion. Finally, we examined whether 5-FC has an inhibitory effect on the functionality of T6SS-5 in vitro using a previously established assay (31) involving strains engineered to constitutively express VirAG, a 2-component regulatory system that normally activates T6SS-5 gene expression in the mammalian cell cytosol (54). On Western blots, we observed a significant decrease in the quantity of Hcp5, the T6SS-5 intertubule subunit protein, secreted into culture supernatants by *Bt* and *Bp* following 5-FC treatment (Fig. 4*I*). In contrast, expression of Hcp5 was not noticeably affected by 5-FC, as demonstrated by equivalent signal intensities in the cell pellet fractions of treated vs. untreated controls (Fig. 4*I*). These results are consistent with an inhibitory effect of 5-FC on the assembly or secretion activity of T6SS-5 and a consequent decrease in the efficiency of cell–cell spread.

Flucytosine Is a Prodrug That Requires Conversion to 5-Fluorouracil and Fluorouridine Monophosphate. The antifungal activity of 5-FC against *Cryptococcus neoformans* and other fungal pathogens is due to the cytotoxicity of its metabolic products, making it a prodrug (51, 55). As summarized in Fig. 5*A*, following uptake by cytosine permease (CodB) and conversion to 5-fluorouracil (5-FU) by cytosine deaminase (CodA), 5-FC metabolism bifurcates into 2 pathways which ultimately result in antifungal activity via inhibition of RNA and DNA synthesis. Orthologous enzymes and pathways are encoded by *Bp* complex species (Fig. 5*A*); however, bacterial growth in vitro is unaffected by 5-FC at concentrations that suppress Hcp5 secretion under identical growth conditions (Fig. 4 *C* and *I*) and abolish plaque formation by intracellular organisms (Fig. 4*B*). Although the reason for the lack of a primary effect on bacterial growth is presently unknown, it nonetheless implies a unique mechanism for the inhibitory activity of 5-FC. To explore this, we examined the roles of key metabolic enzymes and products in the ability of 5-FC to inhibit cell–cell spread.

Pathway 1 (Fig. 5*A*) is involved in the synthesis of pyrimidine nucleotide triphosphates. We found that 25 μM 5-FU, like 5-FC, abolished plaque formation (Fig. 5*B*). Fluorouridine (FUR), an intermediate between 5-FU and fluorouridine monophosphate (FUMP), was minimally inhibitory at 25 μM but fully inhibitory at 50 μM, suggesting a role for pathway 1. This is consistent with a lack of inhibition by fluorodeoxyuridine (FUdR), a pathway 2 intermediate, at concentrations up to 50 μM. We next investigated metabolic genes for critical roles in the activity of 5-FC (Fig. 5*C*), taking advantage of the availability of an arrayed library of transposon insertion mutants in *Bt* (56). Mutations in genes encoding cytosine deaminase (*codA*::$Tn_{\mathbf{T23}}$) or uracil phosphoribosyltransferase (*upp*::$Tn_{\mathbf{T23}}$) conferred partial or complete resistance to 5-FC, respectively, while mutants defective in thymidine phosphorylase (TP, *deoA*::$Tn_{\mathbf{T23}}$) or ribonucleotide reductase (RR, *Bth_II1936*::$Tn_{\mathbf{T23}}$) remained susceptible. The partial sensitivity of the *codA*::$Tn_{\mathbf{T23}}$ strain could be due to residual activity of the mutant enzyme since the transposon insertion is positioned downstream from the active site of the multidomain aminohydrolase (56). Together, these observations suggest that pathway 2 metabolites, FUdR and FdUMP, are not required for inhibition, whereas metabolic conversion to pathway 1 intermediates 5-FU followed by FUMP is critical for the prodrug activity of 5-FC. FUMP or a downstream metabolite, therefore, are the likely inhibitors of T6SS-5-dependent intercellular spread.

Chemical Mutagenesis Screen for 5-FC Resistance Yields Mutations That Accelerate Cell–Cell Spread. To gain further insight into the inhibitory mechanism of 5-FC, we performed a forward genetic screen to identify mutations leading to resistance. WT *Bt* was treated with the DNA alkylating agent ethyl methanesulfonate (EMS). Pooled mutagenized bacteria were then used to infect

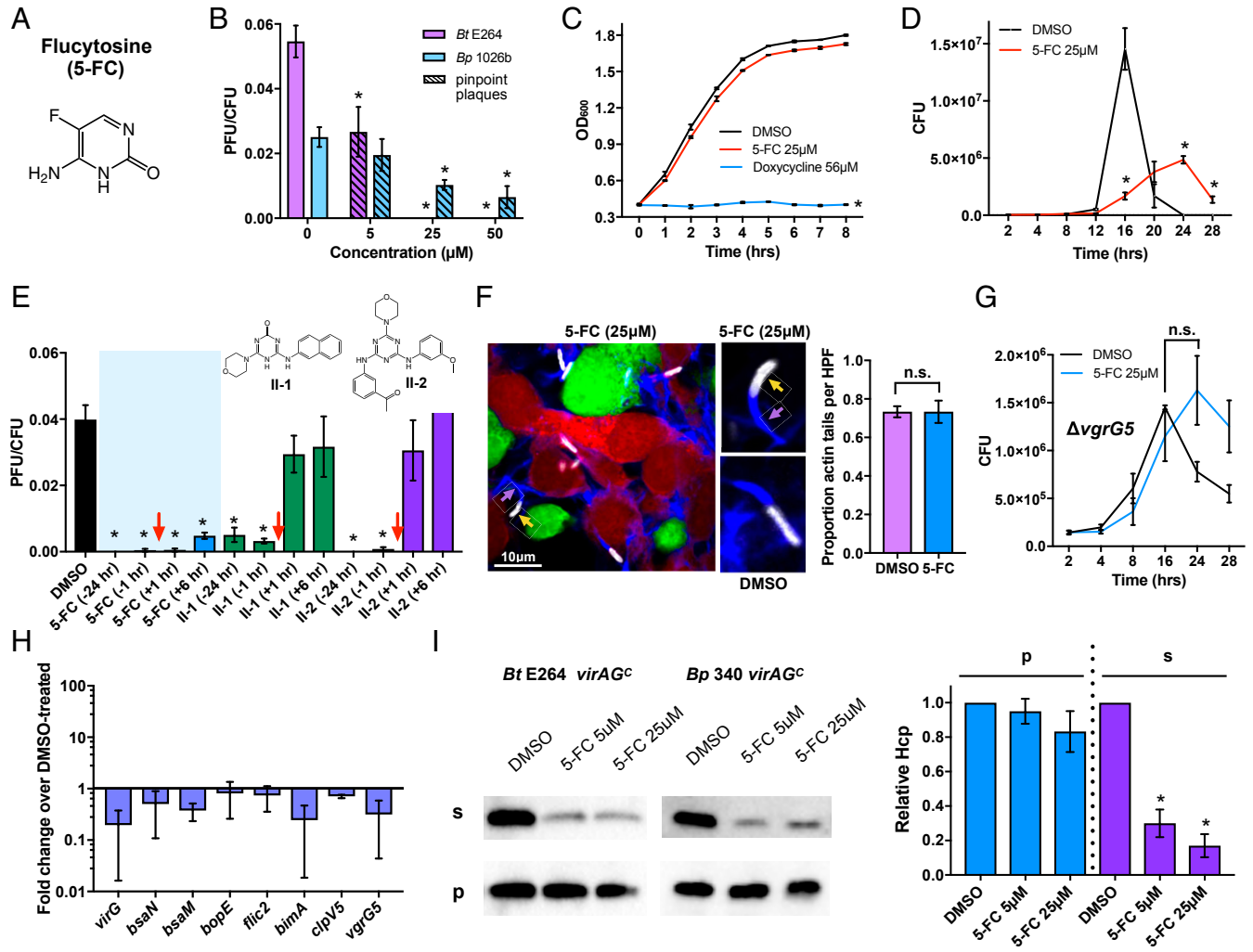

Fig. 4. The FDA-approved antifungal 5-FC inhibits *Burkholderia* intercellular spread and T6SS-5 secretion activity. (*A*) Chemical structure of 5-FC (4-amino-5-fluoro-2(1H)-pyrimidinone). (*B*) Plaque forming efficiency of *Bt* E264 and *Bp* 1026b at increasing concentrations of 5-FC. Flucytosine completely inhibited plaque formation by *Bt* at a concentration of 25 μM. Plaque forming efficiency was assessed by the number of plaque forming units (PFU) per CFU on confluent HEK293 cell monolayers 16 h after infection with a multiplicity of infection (MOI) of 4×10^{-4} (*$P < 0.01$). Striped bars indicate that plaques were pinpoint in size. (*C*) Flucytosine did not significantly inhibit in vitro growth at a concentration that robustly inhibited intercellular spread (25 μM) (*$P < 0.001$). (*D*) Flucytosine delayed and decreased, but did not eliminate, intracellular replication of *Bt* (*$P < 0.05$). Intracellular CFUs were enumerated by treating confluent cell monolayers with 25 μM 5-FC or DMSO, infecting 1 h later with *Bt* at an MOI of 1, adding K_m (1 mg/mL) 1 h after infection to kill extracellular bacteria, then lysing monolayers and plating dilutions at predetermined time points (28, 31). (*E*) Flucytosine at 25 μM robustly inhibited intercellular spread of *Bt* irrespective of time of addition (24 h prior to infection, 1 h prior, 1 h after, and 6 h after), showing that 5-FC blocks a late life cycle step (*$P < 0.001$). This is in contrast to 2 other compounds identified in our screen, which show strong activity when added prior to infection but minimal activity when added after infection. These 2 compounds are designated Invasion Inhibitor-1 (II-1) and Invasion Inhibitor-2 (II-2), and their structures are provided. Red arrows indicate the time of infection. (*F*) Fluorescence microscopy demonstrated that 5-FC at 25 μM does not inhibit actin polymerization (actin, blue, indicated by purple arrow; *Bt*, white, indicated by yellow arrow; HEK293 GFP and RFP-expressing cells, red and green). The histogram shows that equal proportions of DMSO vs. 5-FC–treated intracellular *Bt* expressed actin tails at 9 h after infection. n.s. designates no significant difference ($P = 0.5$). HPF, high-powered field. (*G*) Twenty-five μM 5-FC did not inhibit intracellular replication of a fusion defective mutant (Δ*vgrG5*), as demonstrated by the lack of a significant difference between peak bacterial growth numbers. n.s. designates no significant difference ($P = 0.5$). (*H*) Twenty-five μM 5-FC did not significantly alter expression of *Burkholderia* virulence loci in HEK293 cells, including those belonging to the T6SS-5 gene cluster (*clpV5*, the T6SS-5 AAA-ATPase, or *vgrG5*, the T6SS-5 apparatus tip component), $T3SS_{Bsa}$ (*bsaM*, an apparatus component, and *bopE*, a secreted effector with guanine nucleotide exchange activity (39)), intracellular motility (*bimA*, an actin-nucleating factor required for intracellular motility (40), and *fliC2*, the flagellin component of the Fla2 flagellar system (24)), and virulence regulatory loci (*virG* and *bsaN*). Transcripts were quantified by qRT-PCR. *B*–*H* show the mean and SD of at least 3 technical replicates. (*I*) Flucytosine inhibited secretion of Hcp (supernatant) in both *Bt* E264 and *Bp* 1026b at 5 and 25 μM (*$P < 0.05$) but did not affect expression of Hcp (pellet), indicating that 5-FC inhibits T6SS-5 secretion activity. Hcp levels were measured by densitometry, and shown are the mean and SEM of at least 3 biological replicates. $virAG^c$ indicates constitutive expression of VirAG, the 2-component sensor-regulator that controls expression of T6SS-5, on a chromosomally integrated expression construct. As T6SS-5 is normally only expressed in the host cytosol (53, 54), constitutive VirAG expression activates T6SS-5 transcription in vitro, allowing measurements of secretion activity.

cells in the presence of 25 μM 5-FU (Fig. 6*A*). The use of 5-FU, instead of 5-FC, eliminated selection for mutations in the CodB transporter or the CodA aminohydrolase. MNCs formed by mutagenized bacteria were isolated 16 h postinfection, lysed with detergent, and plated on L-agar for isolation of individual bacterial clones. Resistant phenotypes were validated by plaque assays in the presence of 5-FU. In total, ~6 million chemical mutants containing an average of 8 SNPs per genome were assessed

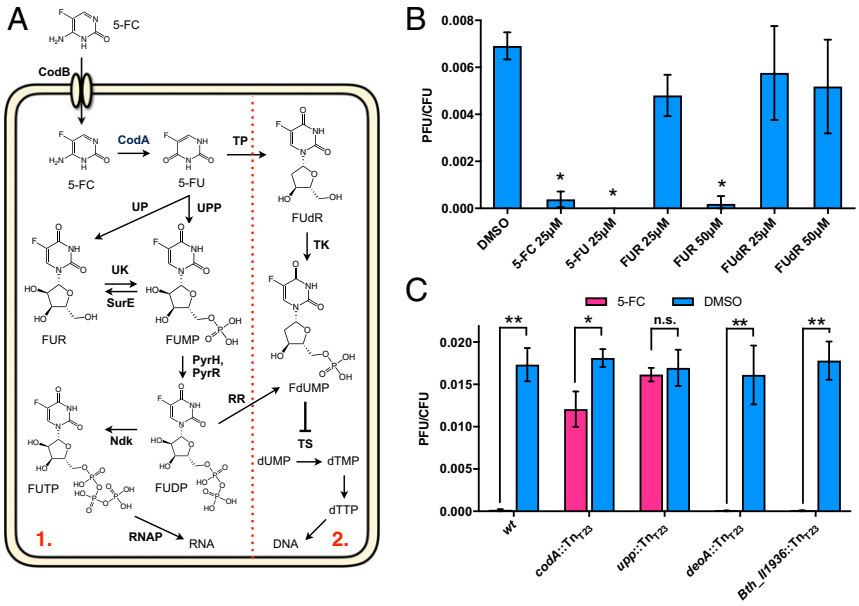

Fig. 5. The inhibitory activity of 5-FC requires metabolic conversion to 5-fluorouracil (5-FU) and fluorouridine monophosphate (FUMP). (*A*) Diagram of 5-FC metabolism in *Burkholderia* (74) based on the presence of gene products homologous to those responsible for metabolic conversion of 5-FC in fungi (55). Flucytosine is metabolized by the pyrimidine salvage pathway. The pathway bifurcates into pathways 1 and 2, which provide nucleotide triphosphate (NTP) and dNTP anabolism and ultimately affect RNA and DNA synthesis, respectively. CodA, cytosine deaminase; CodB, cytosine permease; Ndk, nucleoside diphosphate kinase; PyrH, uridylate kinase; PyrR, bifunctional *pyr* mRNA-binding protein/uracil phosphoribosyltransferase; RNAP, RNA polymerase; RR, ribonucleotide reductase; SurE, 5′/3′-nucleotidase; TK, thymidine kinase; TP, thymidine phosphorylase (DeoA); TS, thymidylate synthase; UK, uridine kinase; UP, uracil phosphorylase; UPP, uracil phosphoribosyltransferase. (*B*) Plaque forming efficiency of *Bt E264* in the presence of 5-FC and its downstream metabolites. Intercellular spread was inhibited by 5-FC; 5-FU; and, at high concentrations, FUR but not by FUdR (*$P < 0.05$). Plaque forming efficiency was assessed by measuring the number of plaque forming units (PFU) per CFU in confluent HEK293 cell monolayers 16 h after infection with a multiplicity of infection of 4×10^{-4}. (*C*) Insertion of transposon Tn_{T23} (56) into *codA* or *upp*, but not *deoA* (encodes TP) or *BTH_II1936* (encodes RR), resulted in resistance to 5-FC at 25 μM, indicating that conversion of 5-FC to 5-FU, and then to FUMP, is essential for the inhibitory effect on *Burkholderia*. Statistical comparisons are for plaque forming efficiency in the DMSO-treated condition vs. the 5-FC treated condition (**$P < 0.01$, *$P < 0.05$, and n.s. = not significant, $P > 0.05$). Shown are the mean and SD of at least 3 technical replicates.

(*SI Appendix*, *Materials and Methods*), and 20 demonstrated reproducible resistance to 5-FU. As detected by PCR amplicon sequencing, 12 of these resistant mutants had a single missense mutation at 1 of 10 different sites in *upp*, and 1 contained a nonsense mutation, validating our results with the *upp*::Tn_{T23} insertion mutant (Fig. 5*C*). No mutations were identified in genes encoding downstream metabolic enzymes PyrH/PyrR or Ndk. The remaining resistant mutants were subjected to whole genome sequencing (WGS) along with the parental WT strain. Since all genomes analyzed contained multiple chemically induced mutations, we searched for genomic regions in which SNPs were identified in more than 1 resistant mutant. Accordingly, 2 regions with clustered SNPs were found (Fig. 6*B*), one containing a pair of regulatory genes which we named Intercellular spread regulators A and B (*isrA* and *isrB*) and another that encodes an array of biosynthetic genes (*thaP*, *thaO*, and adjacent loci) that produce thailandamide, a polyketide antibiotic that inhibits fatty acid biosynthesis by targeting acetyl-coA carboxylase (AccA) (57, 58).

SNP 1 (Fig. 6*B*) is located on chromosome II, 219 bp upstream of the *isrA* coding sequence (CDS) within a region predicted to encode the *isrA* promoter, and SNP 2 lies 80 bp upstream of a small, divergently expressed gene of unknown function (*Bth_II1096*). *isrA* encodes a predicted 28-kDa 2-component response regulator with a winged helix–turn–helix (HTH) DNA-binding domain. Although no apparent sensor gene is located nearby, directly upstream is a second orphan response regulator locus, *isrB*, that encodes a predicted DNA binding protein with a LuxR-type HTH domain. The availability of Tn_{T23} insertions in *isrA* and *isrB* allowed us to assess their roles in susceptibility to 5-FC. In both cases, partial resistance was observed (Fig. 6*C*), with plaques that were uniformly smaller than the *upp*::Tn_{T23} metabolic mutant yet similar to those observed with the original SNP-containing strains. Also located on chromosome II, SNP 3 is a synonymous substitution that falls in the *thaO* coding sequence, which encodes a polyketide synthase required for thailandamide biosynthesis, and SNP 4 results in a Glu to Lys substitution in ThaP, an adjacent polyketide synthase. Although the significance of the synonymous substitution associated with SNP3 was not immediately apparent, the presence of 2 independent SNPs in the thailandamide biosynthetic gene cluster prompted further examination. Indeed, using a *thaP*::Tn_{T8} mutant, we observed partial resistance to 5-FC in plaque assays, similar to that seen with *isrA* and *isrB* mutant strains (Fig. 6*C*).

To our initial surprise, the *isrA* and *thaP* insertion mutants each displayed the striking phenotype of accelerated plaque development in the absence of 5-FC (Fig. 6*D*). For the *isrA*::Tn_{T23} strain, hyper-plaque formation correlated with increased secretion of Hcp5, while the *thaP*::Tn_{T8} mutant showed variable secretion activity. In either case, we propose that factors that normally limit the efficiency of cell–cell spread were inactivated by mutations in chemically mutagenized cells or in independently selected transposon mutants, allowing intracellular *Burkholderia* to partially overcome concentrations of 5-FC that would otherwise abrogate cell–cell spread. The potential basis for the unexpectedly similar phenotypes of mutations in *isrA* and *thaP* and the broader implications of pathways that confer resistance to 5-FC prodrug are considered below (*Discussion*).

BFX and 5-FC Are Efficacious in a Murine Model of Fulminant Melioidosis. Given the effectiveness of BFX and 5-FC at inhibiting *Burkholderia* cell–cell spread, we evaluated their therapeutic efficacy using a mouse model of acute fulminant melioidosis (59). BALB/c mice were infected intranasally with 4,500 CFU of *Bp* 1026b, and BFX (10 mg/kg/day) or 5-FC (100 mg/kg/day) was administered intraperitoneally twice daily, with the first doses given 5 h after infection. Outcomes were compared to animals that were administered placebo (PBS + 20% DMSO) or ceftazidime (130 mg/kg/day), the current antibiotic of choice for treating acute melioidosis. All animals in the placebo group succumbed to infection within 3 d, and all ceftazidime-treated animals succumbed by 5 d postinfection. In contrast, all (100%) of mice receiving BFX and 3/8 (36.7%) mice treated with 5-FC survived 5 d postinfection ($P < 0.001$) (Fig. 7*A*). Moreover, 5/8 (63%) BFX-treated and 1/8 (12%) 5-FC–treated mice survived for the duration of the study (10 d). Survival rates were inversely correlated with bacterial loads in major organs, as numbers of bacteria in the lungs, livers, and spleens of BFX-treated mice were decreased relative to placebo and ceftazidime-treated controls at 48 h postinfection (Fig. 7*B*). Bacterial loads were

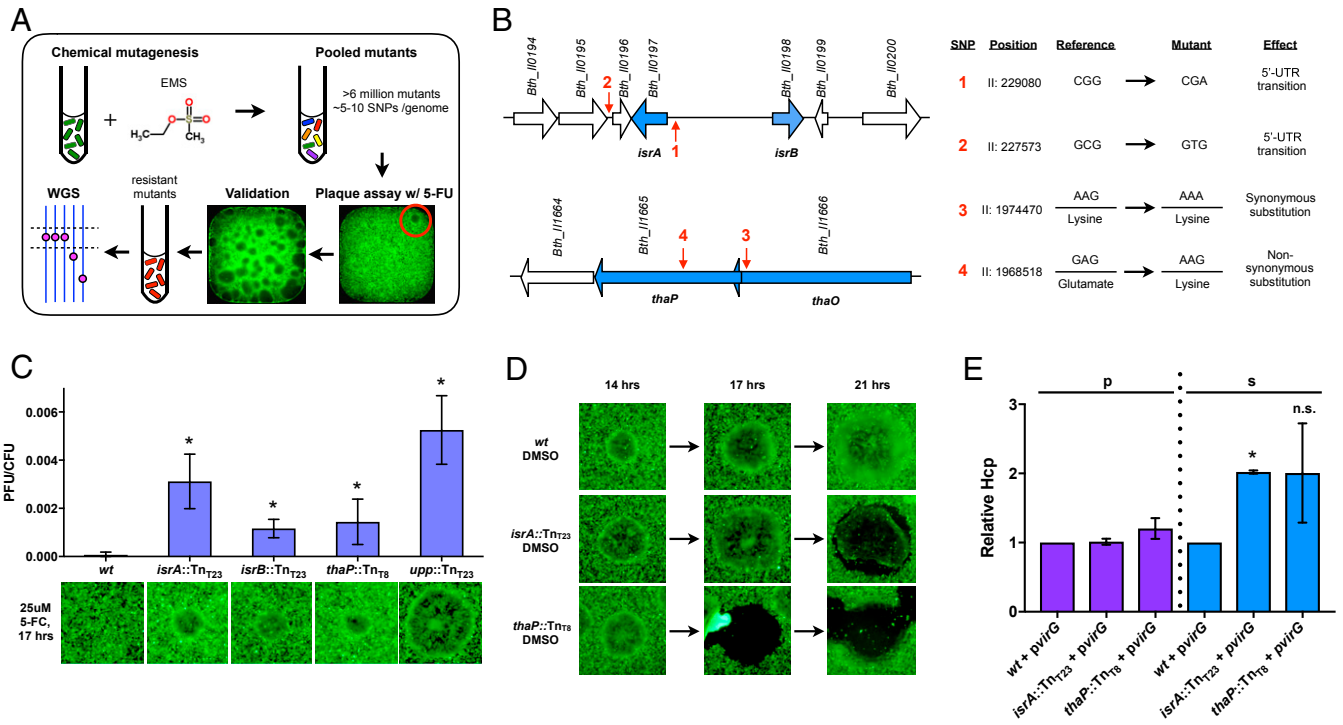

Fig. 6. Flucytosine resistance mutations confer accelerated cell–cell spread. (*A*) Schematic of the forward genetic screen for 5-FC–resistant chemical mutants. WT (*wt*) *Bt* E264 was mutagenized with 1% ethyl methanesulfonate (EMS), and pooled mutants were used to infect confluent cell monolayers in 384-well plates treated with 25 μM 5-FU at a multiplicity of infection of 0.03. MNCs were lysed and plated after 16 h of incubation. Colonies were validated for resistance followed by whole-genome sequencing of resistant clones. (*B*) Mutations clustered in 2 genomic regions: one encoding 2 putative transcriptional response regulators (*isrA* and *isrB*) and the other encoding a polyketide synthase cluster (*thaP*, *thaO*, and adjacent loci). Red arrows indicate the location of SNPs in resistant chemical mutants. SNP 1 is located 219 bp upstream of *isrA* in a potential promoter region; SNP 2 lies in an intergenic region, 80 bp upstream of the coding sequence of an adjacent hypothetical protein *Bth_II0196* within a potential stem-loop sequence of unknown function; SNP 3 creates a synonymous substitution in *thaO*; and SNP 4 results in a nonsynonymous substitution in *thaP*. (*C*) Insertion of transposon Tn_{T23} or Tn_{T8} (56) into *isrA*, *isrB*, or *thaP* also resulted in partial resistance as shown in standard plaque assays with 25 μm 5-FC. A Tn_{T23} insertion in *upp*, for comparison, resulted in more robust resistance ($*P < 0.05$). Shown are the mean and SD of at least 3 technical replicates. (*D*) *isrA* and *thaP* mutants displayed accelerated plaque formation in the absence of 5-FC. (*E*) The *isrA* mutant carrying a plasmid expressing VirG (*isrA*::Tn_{T23} + p*virG*) had consistently increased Hcp secretion (supernatant [s]) but similar Hcp expression (pellet [p]), relative to WT with p*virG* ($*P < 0.01$). *virG* was expressed in *trans* on a replicating plasmid to activate T6SS-5 expression in vitro, allowing assessment of its secretion activity. The *thaP* mutant (*thaP*::Tn_{T8} + p*virG*) displayed variable levels of Hcp secretion that were not statistically different from WT (n.s., $P > 0.05$). The quantity of Hcp was measured relative to *wt* + p*virG* by densitometry, and shown are the mean and SEM of at least 4 biological replicates.

also decreased, although to a lesser extent, in 5-FC–treated mice. Interestingly, the majority of surviving mice treated with 5-FC or BFX showed low or undetectable bacterial loads at 10 d in liver and spleen compared to lung tissue, suggesting that dissemination from the lung to these organs might portend a poor outcome (*SI Appendix*, Fig. S2). Histopathology of pulmonary, hepatic, and splenic tissue from mice killed 48 h after infection revealed significantly reduced inflammation in 5-FC–treated mice relative to PBS-treated and minimal inflammation in organs of BFX-treated mice (Fig. 7*C*). In summary, BFX and 5-FC demonstrate superiority to ceftazidime in a preclinical model of fulminant melioidosis.

Discussion

The goal of this study was to identify small-molecule inhibitors of the *Burkholderia* intercellular life cycle and to evaluate their therapeutic efficacy. Our cell-based phenotypic screen successfully identified inhibitors of intercellular spread by *Bt*, *Bp*, and *Bm*. We determined the mechanism of action of 1 highly potent molecule, BFX, as inhibition of DNA gyrase and link the effect of 5-FC to inhibition of cell–cell spread, most likely at the point of T6SS-5–mediated membrane fusion.

The intracellular and in vivo efficacy of BFX is intriguing given that fluoroquinolones have not generally been found effective for the treatment of melioidosis in animal models or human clinical trials (22). In contrast, our findings argue that BFX holds promise as a countermeasure against *Bp* and other pathogens. In comparison to ciprofloxacin, significantly increased potency of BFX was observed during intracellular but not extracellular growth, suggesting an ability to achieve higher concentrations of active compound in mammalian cells. If true, further study is warranted to determine if this is due to enhanced membrane permeability, a lower isoelectric point and increased activity in acidic compartments such as the phagolysosome (60, 61), or some other mechanism. A comprehensive assessment of BFX's spectrum of activity, particularly against other intracellular pathogens such as *Shigella* and *Salmonella*, may be informative and clinically relevant in this regard. In *Burkholderia* and other gram-negative bacteria, efflux pumps that actively export antibiotics across the bacterial cell envelope are a primary mechanism of fluoroquinolone resistance (26, 62, 63). Thus, it will be of interest to determine if the enhanced relative potency of BFX against intracellular *Burkholderia* provides a means to overcome efflux-mediated resistance to an extent that improves clinical outcomes (8, 64).

Our observation that 5-FC provided a significant survival benefit in a preclinical model of fulminant disease provides a compelling argument for evaluating the potential to repurpose this antifungal as an adjunctive therapy for melioidosis (65). As

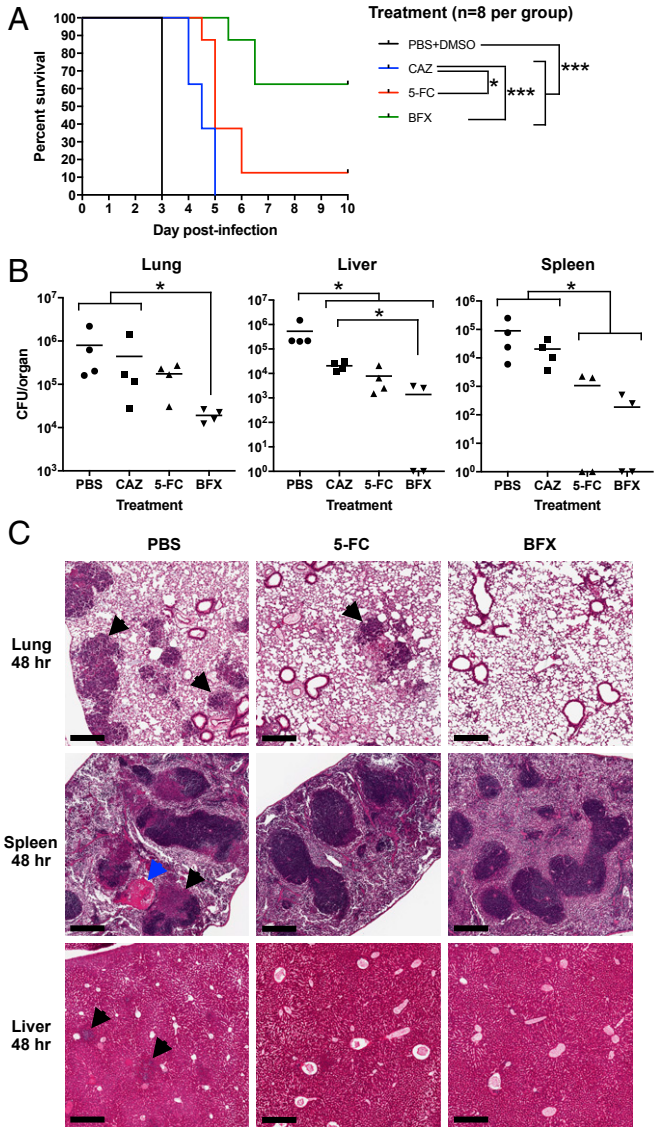

Fig. 7. In vivo efficacy of 5-FC and BFX. (*A*) Treatment of female BALB/c mice with 5-FC and BFX improved survival in a lethal inhalation model of melioidosis and outperformed ceftazidime treatment, the current therapy of choice for acute melioidosis (***$P < 0.001$; *$P < 0.05$). Mice were inoculated intranasally with 4,500 CFU of *Bp* 1026b and treated twice daily, starting 5 h after infection, with either 100 μL of PBS + 20% DMSO (negative control), 65 mg/kg of ceftazidime (positive control), 50 mg/kg of 5-FC, or 5 mg/kg of BFX. Number of mice per group = 8. CAZ, ceftazidime. Animals were euthanized when moribund, as described in *SI Appendix, Supplemental Materials and Methods*. (*B*) Flucytosine and BFX decreased bacterial loads in the lung, liver, and spleen of mice infected with *Bp* 1026b (*$P < 0.05$). Organs were harvested 48 h after infection, and bacterial burden was measured by diluting and plating homogenized organs. Number of mice per group = 4. (*C*) Flucytosine and BFX reduced inflammation and necrosis in the lung, spleen, and liver tissue of infected mice. Shown are lung, spleen, and liver sections from PBS-, 5-FC–, and BFX-treated mice harvested 48 h after infection. PBS-treated mouse lung tissue showed extensive interstitial, perivascular, and peribronchiolar inflammation (black arrows). Inflammation was less prominent and more focal in 5-FC–treated mouse lungs (black arrow) and was absent in BFX-treated lungs. Splenic tissue from PBS-treated mice showed large areas of inflammation (black arrow) and necrosis (blue arrow) within red and white pulp, whereas spleens from 5-FC– and BFX-treated mice were largely spared. Liver tissue from PBS-treated mice showed significant periductal inflammation (black arrows), which was reduced in 5-FC–treated mice and undetectable in BFX-treated mice. All error bars represent the SEM. (Scale bars, 300 μm.)

an FDA-approved drug, 5-FC has a well-established safety and clinical use profile and is readily accessible in many melioidosis-endemic locales. It exhibits excellent bioavailability and near ubiquitous distribution in host compartments, including cerebrospinal fluid (51). In *Burkholderia*, 5-FC acts as a prodrug that requires conversion to 5-FU and FUMP for inhibitory activity. This confers selectivity since human cells lack CodA and cannot efficiently metabolize 5-FC (51). In contrast to susceptible fungi (55), the lack of a primary effect on growth and the lack of dependence on thymidine phosphorylase or ribonucleotide reductase (Fig. 5) suggest that lethal inhibition of RNA or DNA synthesis are not of primary importance. Instead, our staging of the effects of 5-FC in relation to the intracellular life cycle (Fig. 4 *B–J*), the observation that 5-FC suppresses Hcp5 secretion in vitro (Fig. 4*I*), and the phenotypes of resistant mutants (Fig. 6; see below) are consistent with the hypothesis that inhibition of T6SS-5 activity is primarily responsible for the ability of 5-FC to inhibit cell–cell spread. Effects on other requirements for intracellular survival and replication may occur, but our results argue that they are not the primary point of inhibition in the assays we employed.

In our in vitro and cell-based assays, 5-FC acts as an antivirulence agent (66, 67), and targeting virulence as opposed to growth may be advantageous for several reasons. First, antivirulence agents are proposed to exert reduced selective pressure for resistance, although this has been difficult to demonstrate experimentally (66–68). Second, unlike conventional antibiotics which target widely conserved and essential pathways, antivirulence agents typically target pathogen-specific virulence pathways that are dispensable for growth and therefore may be less likely to disrupt beneficial microbes. Moreover, the unique mechanisms of action of antivirulence agents like 5-FC provide opportunities for synergy when combined with established therapies or promising leads such as BFX, which target growth. Further efforts to develop 5-FC will focus in part on its use as an adjunctive therapy to treat melioidosis.

Through chemical and targeted mutagenesis experiments, we have identified 3 general pathways to 5-FC resistance. The first and most efficient involves mutations in genes encoding cytosine deaminase (*codA*) or uracil phosphoribosyltransferase (*upp*), which are required for conversion of 5-FC prodrug to active metabolites, and we anticipate that mutations in the *codB* transporter locus would have a similar effect. Fluorinated pyrimidines have also been found to exert antivirulence effects in *P. aeruginosa*, and although the mechanism remains unclear, disruptions in *codA* and *upp* were similarly found to confer resistance (68, 69). A second pathway that leads to partial resistance results from mutations in a region of chromosome II that encodes putative regulatory factors such as IsrA and IsrB. Although further study is required to understand their roles in virulence, the intriguing observation that a transposon insertion in *isrA* results in accelerated plaque development in the absence of inhibitor suggests that IsrA plays a negative role in regulating 1 or more factors involved in intracellular spread. A third pathway, which also confers partial resistance, involves inactivation of a biosynthetic gene (*thaP*) required for production of thailandamide, a potent inhibitor of acetyl-coA carboxylase (AccA)-dependent fatty acid synthesis (57, 58). How might the lack of production of a polyketide antibiotic increase the efficiency of cell–cell spread? An important clue comes from the observation that in addition to inhibiting growth of competing bacteria (57, 58), thailandamide has cytotoxic activity against mammalian cells (70). We speculate that partial disruption of host cell fatty acid biosynthesis by intracellular bacteria could alter membrane properties and decrease the efficiency of T6SS-5 dependent fusion or compromise mechanisms that repair membrane damage resulting from nonproductive deployment of the fusion machinery. In either case, eliminating thailandamide production

would be predicted to increase the efficiency of cell–cell spread as measured by in vitro plaque assays.

Having identified pathways to 5-FC resistance in vitro, it is important to consider their potential clinical relevance in relation to the ecology and epidemiology of *Bp*. Human infections invariably arise from environmental sources (4), and it seems likely that mutations in genes required for pyrimidine salvage (i.e., *codA*, *codB*, and *upp*) would be subject to negative selection in nature. The effects of such mutations on *Bp* virulence in animals are also unknown. Similarly, although disruption of *isrA* or other potential regulatory loci may increase the efficiency of intercellular spread in cell monolayers, further experiments will be required to determine if this correlates with increased or attenuated virulence in vivo. Given the importance of precise control in bacterial–host interactions, we predict the latter possibility will be true. Finally, although thailandamide is produced by *Bt* strains, the biosynthetic gene cluster is absent from *Bp* and *Bm* genomes (71), making this pathway of lesser relevance for treating melioidosis or glanders. Nonetheless, it is tempting to speculate that inhibition of host cell fatty acid synthesis could contribute to the relative avirulence of *Bt* compared to *Bp* and *Bm*. Although our chemical mutagenesis screen was designed to reveal the mechanism of inhibition by 5-FC, mutations that implicate a specific molecular target were not identified. If 5-FC ultimately targets a factor required for T6SS-5 apparatus assembly, function, or deployment, it may be difficult or impossible to generate mutations in a single step that eliminate inhibition while preserving secretory and fusogenic activity, as dictated by our selection protocol. Similarly, effects on regulatory factors or levels of a small-molecule signal may be difficult to evade without disrupting essential control circuits. Given the apparent utility of 5-FC and the required role of T6SS-5 in pathogenesis, it is clearly of interest to identify the molecular targets and mechanisms responsible for inhibition.

A limitation of our study is that the primary screen was conducted with the BSL-2 surrogate *Bt* for relative ease of manipulation. As we later found, many of our primary hits had no effect on *Bp* or *Bm*. Although *Bt*, *Bp*, and *Bm* utilize many conserved virulence mechanisms, their genomes differ considerably in size, metabolic gene content, and homology (71, 72). Subtle differences in intercellular life cycles, drug uptake or retention, or metabolic strategies of these species may have contributed to the differential susceptibility observed in our study. Although our screen was successful in identifying therapeutic leads for *Bp* and/or *Bm*, a potentially superior but more challenging approach would have been to conduct the primary screen using these Tier 1 pathogens under BSL-3 containment. Finally, our study demonstrated the efficacy of identified hits in clinical isolates; however, follow-on strain surveys will be required to guide translation to the clinical setting, as *Bp* is known to be genetically variable (10).

Cell-based phenotypic screens are a promising approach to drug discovery for intracellular bacterial pathogens, as validated hits will have a priori demonstrated the ability to traverse the host cell plasma membrane and bacterial cell envelope. This is especially advantageous for gram-negative pathogens, for which the outer membrane remains a formidable barrier for drug development (73). The high-throughput screen described here demonstrates the feasibility of this approach to identify new therapeutic leads for melioidosis and glanders.

Materials and Methods

Study Design. Compounds in the UCLA MSSR library (www.mssr.ucla.edu) were plated and tested in vitro for the ability to inhibit intercellular spread with the identities and order of compounds blinded to the experimenter. Due to its scale and expense, the ∼220,000–small-molecule HT screen was performed with each compound tested once in a single well. Small molecules deemed as positive hits in initial screening were cherry-picked from the larger library to form a small positive hit library. This hit library was used to validate positive hits in 384-well format, with at least 3 technical and 2 biological replicates per compound. Downstream cell-based infection experiments were performed with at least 3 technical and 2 biological replicates. Compounds were prioritized for further study based on their activity profiles and toxicity for mammalian cells. Two compounds, BFX and 5-FC, were selected for mechanistic studies, and their therapeutic efficacy was measured in vivo in a mouse model of melioidosis. Animal studies were approved by the University of Florida Institutional Animal Care and Use Committee (IACUC) under protocol #201609601. Animals were randomly assigned to treatment groups, and therapeutic efficacy was determined on the basis of mortality, organ bacterial loads, and histopathological findings. Sample sizes for in vivo studies were determined using Lamorte's power calculations and were selected to minimize the number of animals needed to obtain statistically significant results. The HT small-molecule screen, follow-up mechanistic assays, HT resistance screen, WGS and bioinformatics approach, animal experiments, and data analysis are described in detail in *SI Appendix*.

ACKNOWLEDGMENTS. We thank the members of the J.F.M. laboratory for valuable discussions. We thank undergraduate researchers Minna Ding, Christy Kim, and Anh Huynh (UCLA) for their technical assistance. P.L.B. thanks Steve Smale, Kelsey Martin, Robert Modlin, Marcus Horwitz, Alex Hoffmann, Kent Hill, Ann Hirsch, Elizabeth Neufeld, Atish Ganguly, and Umesh Ahuja for their mentorship. We thank Bart Currie and his group at the Menzies School of Health Research for providing the MSHR305 *Bp* strain. We thank Romney Humphries and the UCLA Clinical Microbiology Laboratory for providing *P. aeruginosa* and *E. coli* strains. We also thank Colin Manoil (University of Washington) for providing us with the *Bt* transposon mutant library. We thank Ken Ng for his artistic guidance and Alexander Sun (California Institute of Technology [Caltech]) for his organic chemistry expertise. This work was supported by the NIH Pacific Southwest Regional Center of Excellence for Biodefense and Emerging Infectious Diseases under award U54 AI065359 to J.F.M. and the Defense Threat Reduction Agency under awards HDTRA1-11-1-003 and HDTRA1-17-1-0015 to J.F.M. and C.T.F. P.L.B. received fellowship support from the National Institute of Allergy and Infectious Diseases of the NIH (F30AI118342), the UCLA–Caltech Medical Scientist Training Program (T32GM008042), and a Paul and Daisy Soros Fellowship for New Americans. H.P.S. was supported by University of Florida Preeminence start-up funds. Animal studies were funded by Emerging Pathogens Institute seed fund award 16-3 to M.H.N.

1. M. Kaestli *et al.*, Out of the ground: Aerial and exotic habitats of the melioidosis bacterium Burkholderia pseudomallei in grasses in Australia. *Environ. Microbiol.* **14**, 2058–2070 (2012).
2. J. L. Ginther *et al.*, Identification of Burkholderia pseudomallei near-neighbor species in the Northern Territory of Australia. *PLoS Negl. Trop. Dis.* **9**, e0003892 (2015).
3. B. J. Currie, M. Kaestli, Epidemiology: A global picture of melioidosis. *Nature* **529**, 290–291 (2016).
4. W. J. Wiersinga *et al.*, Melioidosis. *Nat. Rev. Dis. Primers* **4**, 17107 (2018).
5. L. B. Randall, K. Dobos, K. M. Papp-Wallace, R. A. Bonomo, H. P. Schweizer, Membrane-bound PenA β-Lactamase of Burkholderia pseudomallei. *Antimicrob. Agents Chemother.* **60**, 1509–1514 (2015).
6. N. L. Podnecky, V. Wuthiekanun, S. J. Peacock, H. P. Schweizer, The BpeEF-OprC efflux pump is responsible for widespread trimethoprim resistance in clinical and environmental Burkholderia pseudomallei isolates. *Antimicrob. Agents Chemother.* **57**, 4381–4386 (2013).
7. H. P. Schweizer, Mechanisms of antibiotic resistance in Burkholderia pseudomallei: Implications for treatment of melioidosis. *Future Microbiol.* **7**, 1389–1399 (2012).
8. K. A. Rhodes, H. P. Schweizer, Antibiotic resistance in Burkholderia species. *Drug Resist. Updat.* **28**, 82–90 (2016).
9. W. J. Wiersinga, B. J. Currie, S. J. Peacock, Melioidosis. *N. Engl. J. Med.* **367**, 1035–1044 (2012).
10. C. Chewapreecha *et al.*, Global and regional dissemination and evolution of Burkholderia pseudomallei. *Nat. Microbiol.* **2**, 16263 (2017).
11. K. E. Van Zandt, M. T. Greer, H. C. Gelhaus, Glanders: An overview of infection in humans. *Orphanet J. Rare Dis.* **8**, 131 (2013).
12. A. Srinivasan *et al.*, Glanders in a military research microbiologist. *N. Engl. J. Med.* **345**, 256–258 (2001).
13. R. Stone, Infectious disease. Racing to defuse a bacterial time bomb. *Science* **317**, 1022–1024 (2007).
14. D. A. Dance, "Melioidosis and glanders as possible biological weapons" in *Bioterrorism and Infectious Agents* (Springer Science, New York, 2005), pp. 99–145.
15. L. A. Morici, J. Heang, T. Tate, P. J. Didier, C. J. Roy, Differential susceptibility of inbred mouse strains to Burkholderia thailandensis aerosol infection. *Microb. Pathog.* **48**, 9–17 (2010).
16. A. Sawana, M. Adeolu, R. S. Gupta, Molecular signatures and phylogenomic analysis of the genus Burkholderia: Proposal for division of this genus into the emended genus Burkholderia containing pathogenic organisms and a new genus Paraburkholderia gen. nov. harboring environmental species. *Front. Genet.* **5**, 429 (2014).

17. A. Haraga, T. E. West, M. J. Brittnacher, S. J. Skerrett, S. I. Miller, Burkholderia thailandensis as a model system for the study of the virulence-associated type III secretion system of Burkholderia pseudomallei. *Infect. Immun.* **76**, 5402–5411 (2008).
18. D. Limmathurotsakul *et al*., Predicted global distribution of Burkholderia pseudomallei and burden of melioidosis. *Nat. Microbiol.* **1**, 15008 (2016).
19. B. J. Currie, L. Ward, A. C. Cheng, The epidemiology and clinical spectrum of melioidosis: 540 cases from the 20 year Darwin prospective study. *PLoS Negl. Trop. Dis.* **4**, e900 (2010).
20. B. Maharjan *et al*., Recurrent melioidosis in patients in northeast Thailand is frequently due to reinfection rather than relapse. *J. Clin. Microbiol.* **43**, 6032–6034 (2005).
21. D. Limmathurotsakul *et al*., Increasing incidence of human melioidosis in Northeast Thailand. *Am. J. Trop. Med. Hyg.* **82**, 1113–1117 (2010).
22. D. Dance, Treatment and prophylaxis of melioidosis. *Int. J. Antimicrob. Agents* **43**, 310–318 (2014).
23. N. L. Podnecky *et al*., Mechanisms of resistance to folate pathway inhibitors in *Burkholderia pseudomallei*: Deviation from the norm. *MBio* **8**, e01357-17 (2017).
24. D. S. Sarovich *et al*., Raising the stakes: Loss of efflux pump regulation decreases meropenem susceptibility in Burkholderia pseudomallei. *Clin. Infect. Dis.* **67**, 243–250 (2018).
25. J. E. Cummings, R. A. Slayden, Transient in vivo resistance mechanisms of Burkholderia pseudomallei to ceftazidime and molecular markers for monitoring treatment response. *PLoS Negl. Trop. Dis.* **11**, e0005209 (2017).
26. N. L. Podnecky, K. A. Rhodes, H. P. Schweizer, Efflux pump-mediated drug resistance in Burkholderia. *Front. Microbiol.* **6**, 305 (2015).
27. M. N. Burtnick *et al*., Burkholderia pseudomallei type III secretion system mutants exhibit delayed vacuolar escape phenotypes in RAW 264.7 murine macrophages. *Infect. Immun.* **76**, 2991–3000 (2008).
28. C. T. French *et al*., Dissection of the Burkholderia intracellular life cycle using a photothermal nanoblade. *Proc. Natl. Acad. Sci. U.S.A.* **108**, 12095–12100 (2011).
29. M. P. Stevens *et al*., Identification of a bacterial factor required for actin-based motility of Burkholderia pseudomallei. *Mol. Microbiol.* **56**, 40–53 (2005).
30. E. E. Galyov, P. J. Brett, D. DeShazer, Molecular insights into Burkholderia pseudomallei and Burkholderia mallei pathogenesis. *Annu. Rev. Microbiol.* **64**, 495–517 (2010).
31. I. J. Toesca, C. T. French, J. F. Miller, The type VI secretion system spike protein VgrG5 mediates membrane fusion during intercellular spread by pseudomallei group Burkholderia species. *Infect. Immun.* **82**, 1436–1444 (2014).
32. S. Schwarz *et al*., VgrG-5 is a Burkholderia type VI secretion system-exported protein required for multinucleated giant cell formation and virulence. *Infect. Immun.* **82**, 1445–1452 (2014).
33. S. Schwarz *et al*., Burkholderia type VI secretion systems have distinct roles in eukaryotic and bacterial cell interactions. *PLoS Pathog.* **6**, e1001068 (2010).
34. R. Milde *et al*., Multinucleated giant cells are specialized for complement-mediated phagocytosis and large target destruction. *Cell Rep.* **13**, 1937–1948 (2015).
35. M. Brackmann, S. Nazarov, J. Wang, M. Basler, Using force to punch holes: Mechanics of contractile nanomachines. *Trends Cell Biol.* **27**, 623–632 (2017).
36. M. Basler, J. J. Mekalanos, Type 6 secretion dynamics within and between bacterial cells. *Science* **337**, 815 (2012).
37. S. Pukatzki, A. T. Ma, A. T. Revel, D. Sturtevant, J. J. Mekalanos, Type VI secretion system translocates a phage tail spike-like protein into target cells where it cross-links actin. *Proc. Natl. Acad. Sci. U.S.A.* **104**, 15508–15513 (2007).
38. S. Pukatzki *et al*., Identification of a conserved bacterial protein secretion system in Vibrio cholerae using the Dictyostelium host model system. *Proc. Natl. Acad. Sci. U.S.A.* **103**, 1528–1533 (2006).
39. M. Basler, M. Pilhofer, G. P. Henderson, G. J. Jensen, J. J. Mekalanos, Type VI secretion requires a dynamic contractile phage tail-like structure. *Nature* **483**, 182–186 (2012).
40. L. Whiteley *et al*., Entry, intracellular survival, and multinucleated-giant-cell-forming activity of Burkholderia pseudomallei in human primary phagocytic and nonphagocytic cells. *Infect. Immun.* **85**, 1–12 (2017).
41. S. Pilatz *et al*., Identification of Burkholderia pseudomallei genes required for the intracellular life cycle and in vivo virulence. *Infect. Immun.* **74**, 3576–3586 (2006).
42. V. Hopf *et al*., BPSS1504, a cluster 1 type VI secretion gene, is involved in intracellular survival and virulence of Burkholderia pseudomallei. *Infect. Immun.* **82**, 2006–2015 (2014).
43. M. N. Burtnick *et al*., The cluster 1 type VI secretion system is a major virulence determinant in Burkholderia pseudomallei. *Infect. Immun.* **79**, 1512–1525 (2011).
44. D. J. Payne, M. N. Gwynn, D. J. Holmes, D. L. Pompliano, Drugs for bad bugs: Confronting the challenges of antibacterial discovery. *Nat. Rev. Drug Discov.* **6**, 29–40 (2007).
45. K. Lewis, Platforms for antibiotic discovery. *Nat. Rev. Drug Discov.* **12**, 371–387 (2013).
46. B. Spellberg, D. N. Gilbert, The future of antibiotics and resistance: A tribute to a career of leadership by John Bartlett. *Clin. Infect. Dis.* **59** (suppl. 2), S71–S75 (2014).
47. D. M. Estes, S. W. Dow, H. P. Schweizer, A. G. Torres, Present and future therapeutic strategies for melioidosis and glanders. *Expert Rev. Anti Infect. Ther.* **8**, 325–338 (2010).
48. H. Koga, A. Itoh, S. Murayama, S. Suzue, T. Irikura, Structure-activity relationships of antibacterial 6,7- and 7,8-disubstituted 1-alkyl-1,4-dihydro-4-oxoquinoline-3-carboxylic acids. *J. Med. Chem.* **23**, 1358–1363 (1980).
49. K. Araki *et al*., Quinolone antimicrobial agents substituted with morpholines at the 7-position. Syntheses and structure-activity relationships. *J. Med. Chem.* **36**, 1356–1363 (1993).
50. S. Bazile, N. Moreau, D. Bouzard, M. Essiz, Relationships among antibacterial activity, inhibition of DNA gyrase, and intracellular accumulation of 11 fluoroquinolones. *Antimicrob. Agents Chemother.* **36**, 2622–2627 (1992).
51. J. E. Nett, D. R. Andes, Antifungal agents: Spectrum of activity, pharmacology, and clinical indications. *Infect. Dis. Clin. North Am.* **30**, 51–83 (2016).
52. WHO, "WHO model list of essential medicines" in *Essential Medicines and Health Products*, (World Health Organization, Geneva, Switzerland, 2017), pp. 17–18.
53. Y. Chen *et al*., Characterization and analysis of the Burkholderia pseudomallei BsaN virulence regulon. *BMC Microbiol.* **14**, 206 (2014).
54. J. Wong, Y. Chen, Y. H. Gan, Host cytosolic glutathione sensing by a membrane histidine kinase activates the type VI secretion system in an intracellular bacterium. *Cell Host Microbe* **18**, 38–48 (2015).
55. A. Vermes, H. J. Guchelaar, J. Dankert, Flucytosine: A review of its pharmacology, clinical indications, pharmacokinetics, toxicity and drug interactions. *J. Antimicrob. Chemother.* **46**, 171–179 (2000).
56. L. A. Gallagher *et al*., Sequence-defined transposon mutant library of Burkholderia thailandensis. *MBio* **4**, e00604–e00613 (2013).
57. C. E. Wozniak, Z. Lin, E. W. Schmidt, K. T. Hughes, T. G. Liou, Thailandamide, a fatty acid synthesis antibiotic that is coexpressed with a resistant target gene. *Antimicrob. Agents Chemother.* **62**, 1–14 (2018).
58. Y. Wu, M. R. Seyedsayamdost, The polyene natural product thailandamide A inhibits fatty acid biosynthesis in Gram-positive and Gram-Negative bacteria. *Biochemistry* **57**, 4247–4251 (2018).
59. K. Amemiya *et al*., Comparison of the early host immune response to two widely diverse virulent strains of Burkholderia pseudomallei that cause acute or chronic infections in BALB/c mice. *Microb. Pathog.* **86**, 53–63 (2015).
60. A. Dalhoff, S. Schubert, A. Vente, Pharmacodynamics of finafloxacin, ciprofloxacin, and levofloxacin in serum and urine against TEM- and SHV-type extended-spectrum-β-lactamase-producing enterobacteriaceae isolates from patients with urinary tract infections. *Antimicrob. Agents Chemother.* **61**, 1–10 (2017).
61. K. B. Barnes *et al*., Demonstrating the protective efficacy of the novel fluoroquinolone finafloxacin against an inhalational exposure to Burkholderia pseudomallei. *Antimicrob. Agents Chemother.* **61**, 1–17 (2017).
62. D. V. Viktorov *et al*., High-level resistance to fluoroquinolones and cephalosporins in Burkholderia pseudomallei and closely related species. *Trans. R. Soc. Trop. Med. Hyg.* **102** (suppl. 1), S103–S110 (2008).
63. G. A. Jacoby, Mechanisms of resistance to quinolones. *Clin. Infect. Dis.* **41** (suppl. 2), S120–S126 (2005).
64. W. Chaowagul, Y. Suputtamongkul, M. D. Smith, N. J. White, Oral fluoroquinolones for maintenance treatment of melioidosis. *Trans. R. Soc. Trop. Med. Hyg.* **91**, 599–601 (1997).
65. M. A. Farha, E. D. Brown, Drug repurposing for antimicrobial discovery. *Nat. Microbiol.* **4**, 565–577 (2019).
66. B. K. Johnson, R. B. Abramovitch, Small molecules that sabotage bacterial virulence. *Trends Pharmacol. Sci.* **38**, 339–362 (2017).
67. D. A. Rasko, V. Sperandio, Anti-virulence strategies to combat bacteria-mediated disease. *Nat. Rev. Drug Discov.* **9**, 117–128 (2010).
68. F. Imperi, E. V. Fiscarelli, D. Visaggio, L. Leoni, P. Visca, Activity and impact on resistance development of two antivirulence fluoropyrimidine drugs in *Pseudomonas aeruginosa*. *Front. Cell. Infect. Microbiol.* **9**, 49 (2019).
69. D. R. Kirienko, A. V. Revtovich, N. V. Kirienko, A. High-Content, A high-content, phenotypic screen identifies fluorouridine as an inhibitor of pyoverdine biosynthesis and Pseudomonas aeruginosa virulence. *MSphere* **1**, e00217-16 (2016).
70. K. Ishida, T. Lincke, S. Behnken, C. Hertweck, Induced biosynthesis of cryptic polyketide metabolites in a Burkholderia thailandensis quorum sensing mutant. *J. Am. Chem. Soc.* **132**, 13966–13968 (2010).
71. C. D. Majerczyk *et al*., Cross-species comparison of the Burkholderia pseudomallei, Burkholderia thailandensis, and Burkholderia mallei quorum-sensing regulons. *J. Bacteriol.* **196**, 3862–3871 (2014).
72. L. Losada *et al*., Continuing evolution of Burkholderia mallei through genome reduction and large-scale rearrangements. *Genome Biol. Evol.* **2**, 102–116 (2010).
73. J. Cama, A. M. Henney, M. Winterhalter, Breaching the barrier: Quantifying antibiotic permeability across Gram-negative bacterial membranes. *J. Mol. Biol.* 10.1016/j.jmb.2019.03.031 (2019).
74. KEGG, Pyrimidine metabolism- Burkholderia thailandensis E264. https://www.genome.jp/dbget-bin/www_bget?bte00240. Accessed 31 August 2016.